

## Detailed characteristic comparison between planar and MOLB-type SOFCs

J.J. Hwang<sup>a,\*</sup>, C.K. Chen<sup>b</sup>, D.Y. Lai<sup>b</sup>

<sup>a</sup> *Research Center for Advanced Science and Technology, Mingdao University, Peetou, Changhua 52345, Taiwan, ROC*

<sup>b</sup> *Department of Mechanical Engineering, National Cheng Kung University, Tainan 701, Taiwan*

Received 24 October 2004; accepted 18 November 2004

Available online 8 February 2005

### Abstract

Detailed comparisons of fluid flow, concentration, and electric fields between the planar solid oxide fuel cell (planar SOFC) and the mono-block-layer-built solid oxide fuel cell (MOLB-type SOFC) are made in the present study. A multi-physics model is developed to simulate the SOFCs of different geometries. The model couples the electrochemical kinetics with the fluid dynamics and multi-component species transport. Darcy's law governs the flow momentum in the porous electrodes. The Bruggeman model depicts the diffusion of reactant species within the electrodes. The electrochemical kinetics and the species transport on the electrode surfaces is connected by the Butler–Volmer equation. Results show that the MOLB-type SOFC has a higher fuel/oxidant utilization than the planar SOFC. The high utilization of the fuel/oxidant reflects the high current through the SOFC.

© 2004 Elsevier B.V. All rights reserved.

*Keywords:* MOLB; SOFC; Transport

### 1. Introduction

The solid oxide fuel cell (SOFC) is a potential candidate for future energy conversion schemes because of its higher conversion efficiency than the conventional heat engine. Besides, internal reforming of hydrocarbon fuels can be performed at the anode, which allows direct use of natural gas, LPG, and methanol as fuels. Underlying such projected benefits are its fuel flexibility and higher efficiency compared to the conventional energy conversion system such as ICES.

There is a large amount of research on SOFCs. Focus has been placed on the designs of new material [1–4] and/or novel geometry [5–8]. The planar SOFC has received much more attention than the tubular SOFC because of its easier fabrication and higher power density. Fig. 1(a) schematically shows a typical planar SOFC. PEN (posi-

tive electrode–electrolyte–negative electrode) plate is sandwiched between two inter-connectors (bipolar plates). The inter-connectors are machined with passages for channeling the fuel and air to the fuel cell. Fig. 1(b) shows another geometry known as the MOLB (mono-block-layer-built)-type SOFC. The PEN plate is molded into a corrugated shape. The fuel and air run in the trapezoidal channels that are separated by the corrugated PEN plate. Since the inter-connectors are flat, the laborious work of channel machining is not necessary.

The objective of the present study is to compare the transport and electrochemical characteristics between the conventional planar SOFC and the MOLB-type SOFC. A CFD-based, multi-physics, and electrochemical-transport coupled SOFC model is developed. The model involves solving conservation equations for mass, momentum, energy, multi-component species, and electrical charge along with electrochemical kinetics both in the active and inactive regions of the SOFC. The results obtained by this study can assist the designer in understanding how geometry affects gas transport and electrochemical characteristics in the SOFC. Also,

\* Corresponding author. Tel.: +886 48876660x8302; fax: +886 422518272.

E-mail address: [azaijj@mdu.edu.tw](mailto:azaijj@mdu.edu.tw).

## Nomenclature

$a'$	stoichiometric coefficient of the products
$a''$	stoichiometric coefficient of the reactants
$D$	diffusivity [ $\text{m}^2 \text{s}^{-1}$ ]
$F$	Faraday's constant [ $96487 \text{ C mol}^{-1}$ ]
$\mathbf{i}$	current density [ $\text{A m}^{-2}$ ]
$\mathbf{j}$	transfer current density [ $\text{A m}^{-3}$ ]
$\mathbf{J}$	diffusive flux [ $\text{kg s}^{-1} \text{m}^{-2}$ ]
$k$	thermal conductivity [ $\text{W K}^{-1} \text{m}^{-1}$ ]
$M$	molecular weight [ $\text{kg mol}^{-1}$ ]
$p$	pressure [Pa]
$p_i$	possibility of the same particles stretch from the inter-connector to the electrolyte
$R$	universal gas constant [ $\text{W mol}^{-1} \text{K}^{-1}$ ]
$T$	temperature [K]
$\mathbf{U}$	velocity vectors [ $\text{m s}^{-1}$ ]
$X, Y, Z$	coordinate system, Fig. 1 [m]
$X_i$	fraction of molar concentration of species $i$
$Y_i$	mass fraction of species of $i$

### Greek symbols

$\alpha$	symmetric factor
$\varepsilon$	porosity
$\eta$ (or Over_P)	overpotential, $\Phi_C - \Phi_E$ [V]
$\kappa$	permeability [ $\text{m}^2$ ]
$\mu$	viscosity [ $\text{m s}^{-2}$ ]
$\rho$	density [ $\text{kg m}^3$ ]
$\sigma$	electric conductivity [ $\Omega^{-1} \text{m}^{-1}$ ]
$\tau$	tortuosity of the porous electrode
$\Phi$	solid-phase potential [V]

### Subscripts

A	anode
C	catalyst or cathode
eff	effective
E	electrolyte
F	fluid
$i$	species
ref	reference
S	solid
T	transfer current

they can provide a more complete basis for optimizing the geometry of the SOFC stack.

## 2. Modelling

### 2.1. Basics of SOFC

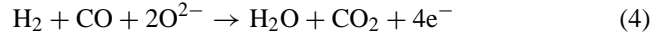
The oxygen reduction reaction on the porous cathode (LSM/YSZ) of the SOFC is



The oxygen ion moves to the anode (nickel/YSZ) through the electrolyte (YSZ). It then reacts with either  $\text{H}_2$  or  $\text{CO}$  on Ni catalysts, i.e.:



The co-oxidations of Eqs. (2) and (3) are currently limited to a single-step reaction, i.e.:



### 2.2. Model equations

The PEN plate is a porous medium, while the flow channels are filled with reactant gases only. In this model, the entire domain is treated as a porous matrix with proper porosities assigned to each sub-domain. For example, the porosity of the open channel is set to 1, and extremely small values of porosity are assigned to the electrolyte and inter-connectors. As a result, the entire domain can be governed by a single set of equations. Thus, it is not necessary to specify the boundary conditions at the interfaces between sub-domains.

#### 2.2.1. Gas-phase transport and reaction

The mass and momentum conservations are described as the following equations:

$$\nabla \cdot (\varepsilon \rho \mathbf{U}) = 0 \quad (5)$$

$$\nabla \cdot (\varepsilon \rho \mathbf{U} \mathbf{U}) = -\varepsilon \nabla p + \nabla \cdot (\varepsilon \mu_{\text{eff}} \nabla \mathbf{U}) + \frac{\varepsilon^2 \mu \mathbf{U}}{\kappa} \quad (6)$$

As for the energy conservation, it is assumed that the fluid and solid phases are in local thermal-equilibrium, and thus the thermal dispersion is negligible. In addition, the thermo-physical properties of both solid and fluid are constant. The equation governing the energy conservation is expressed as

$$\nabla \cdot (\varepsilon \rho C_p \mathbf{U} T) = \nabla \cdot (k_{\text{eff}} \nabla T) - \mathbf{j}_T \cdot \boldsymbol{\eta} + \frac{\mathbf{i} \cdot \mathbf{i}}{\sigma_{\text{eff}}} \quad (7)$$

In the above equation, the radiation heat flux and energy dissipation due to the shear stress are neglected. The effective thermal conductivity can be determined by the following equation [9]:

$$k_{\text{eff}} = -2k_S + \frac{1}{(\varepsilon/(2k_S + k_F)) + ((1 - \varepsilon)/3k_S)} \quad (8)$$

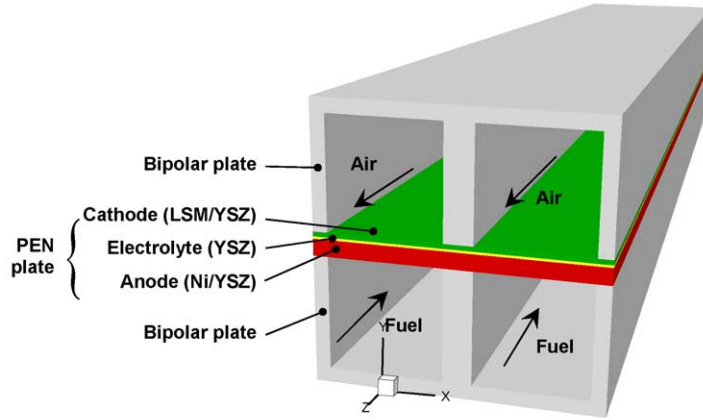
where  $k_F$  is the fluid-phase conductivity, and  $k_S$  the weight-averaged conductivity between the ionic conductor and the electric conductor. The last two terms of Eq. (7) represent the effects of conversion loss and joule heating, respectively.

The conservation of species is expressed as

$$\nabla \cdot (\varepsilon \rho \mathbf{U} Y_i) = \nabla \cdot \mathbf{J}_i + (a_i'' - a_i') \frac{\mathbf{j}_T}{F} \quad (9)$$

$a_i''$  and  $a_i'$  are the stoichiometric coefficients of the products and reactants, respectively. The diffusive mass flux of the

(a) planar SOFC



(b) MOLB-type SOFC

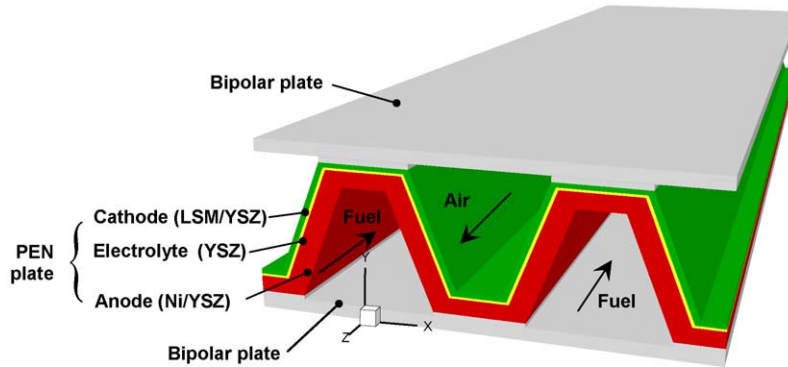


Fig. 1. Schematic drawing of the planar and MOLB-type SOFCs.

species  $\mathbf{J}_i$  is modeled as

$$\mathbf{J}_i = \rho D_{i,\text{eff}} \nabla Y_i + \frac{\rho Y_i}{M} D_{i,\text{eff}} \nabla M - M \sum_j D_{j,\text{eff}} \nabla Y_j - \nabla M \sum_j D_{j,\text{eff}} Y_j \quad (10)$$

The first term on the right-hand side represents the Fickian diffusion due to concentration gradient. The last three terms

are the corrections to enforce the Stefan–Maxwell equations for the multi-component diffusion system. The effective diffusivities in a multi-component mixture of the porous layers follow the Bruggman model [10]:

$$D_{i,\text{eff}} = \varepsilon^\tau D_i \quad (11)$$

The relationship between the electrochemistry and the species transport kinetics on the electrode surfaces is depicted by the Butler–Volmer equation [11]. That is, the transfer cur-

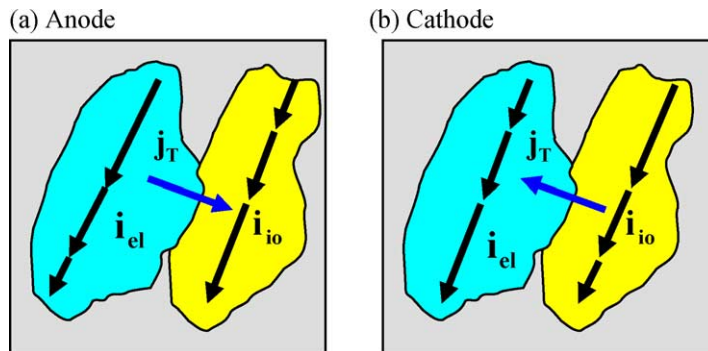


Fig. 2. Current transports in the electrode of the SOFC.

rent densities in the anode and cathode, respectively, are:

$$\mathbf{j}_{T,A} = \mathbf{j}_{0,A} \left\{ \left( \frac{X_{H_2}}{X_{H_2,ref}} \right)^{1/4} \left( \frac{X_{CO}}{X_{CO,ref}} \right)^{1/4} \exp \left[ \frac{\alpha_A F}{RT} \eta \right] - \left( \frac{X_{H_2O}}{X_{H_2O,ref}} \right)^{-1/4} \left( \frac{X_{CO_2}}{X_{CO_2,ref}} \right)^{-1/4} \times \exp \left[ \frac{-(1 - \alpha_A) F}{RT} \eta \right] \right\} \quad (12)$$

$$\mathbf{j}_{T,C} = \mathbf{j}_{0,C} \left( \frac{X_{O_2}}{X_{O_2,ref}} \right)^{1/4} \exp \left( \frac{-\alpha_C F}{RT} \eta \right) \quad (13)$$

where  $\mathbf{j}_0$  is the exchange current density,  $\eta$  the electrode overpotential,  $\alpha_A$  and  $\alpha_C$  the anode and cathode Tafel constants, respectively.

### 2.2.2. Solid-phase conduction

The porous electrode of the SOFC contains two kinds of solid-phase material, i.e., electrolyte (ionic conductor, e.g.

Table 1

Geometric comparison between the planar and MOLB-type SOFCs

Component	Parameters	Planar SOFC	MOLB-type SOFC
Anode	Thickness (mm)	1.4	1.4
	Length (mm)	12	16.8
Electrolyte	Thickness (mm)	0.2	0.2
	Length (mm)	12	16.8
Cathode	Thickness (mm)	0.4	0.4
	Length (mm)	12	16.8
Fuel channel	Cross-sectional area (mm <sup>2</sup> )	90.24	89.6
	Length (mm)	100	100
Air channel	Cross-sectional area (mm <sup>2</sup> )	90.24	89.6
	Length (mm)	100	100
Module	Volume (mm <sup>3</sup> )	28000	28300

YSZ) and catalyst (electric conductor, e.g., LSM or Ni). A potential difference exists between the catalyst ( $\Phi_C$ ) and electrolyte ( $\Phi_E$ ) to drive the transfer current ( $\mathbf{j}_T$ ), keeping the electrochemical reaction continuously. As shown in Fig. 2,

Table 2

Porous-electrochemical properties of the electrodes

Description		Unit	Value
Exchange current	Anode, $\mathbf{j}_{0,A}$	A m <sup>-3</sup>	$1.0 \times 10^9$
	Cathode, $\mathbf{j}_{0,C}$	A m <sup>-3</sup>	$5.0 \times 10^7$
Transfer coefficient	Anode, $\alpha_A$	–	1.0
	Cathode, $\alpha_C$	–	1.0
Porosity, $\varepsilon$	Anode	–	0.4
	Cathode	–	0.5
	Electrolyte	–	$1.0 \times 10^{-5}$
Permeability, $\kappa$	Anode	m <sup>2</sup>	$1.0 \times 10^{-12}$
	Cathode	m <sup>2</sup>	$1.0 \times 10^{-12}$
	Electrolyte	m <sup>2</sup>	$1.0 \times 10^{-18}$
Tortuosity, $\tau$	Anode	–	1.5
	Cathode	–	1.5
	Electrolyte	–	6.0
Effective electric conductivity, $\sigma_{eff}$	Anode	$\Omega^{-1} m^{-1}$	$1.0 \times 10^5$
	Cathode	$\Omega^{-1} m^{-1}$	$7.7 \times 10^3$
	Electrolyte	$\Omega^{-1} m^{-1}$	$1.0 \times 10^{-20}$
Inlet pressure	Anode	kPa	$1.013 \times 10^5$
	Cathode	kPa	$1.013 \times 10^5$
Stack temperature	Anode	K	973
	Cathode	K	973
Mass flow rate	Anode	kg s <sup>-1</sup>	$1.19 \times 10^{-6}$
	Cathode	kg s <sup>-1</sup>	$2.98 \times 10^{-5}$
Species molar concentration at anode inlet	Hydrogen, $X_{H_2}$	–	45.57%
	Carbon monoxide, $X_{CO}$	–	6.97%
	Carbon dioxide, $X_{CO_2}$	–	6.55%
	Water, $X_{H_2O}$	–	36.84%
	Methane, $X_{CH_4}$	–	4.07%
	Total	–	100%
Species molar concentration at cathode inlet	Oxygen, $X_O$	–	21.11%
	Nitrogen, $X_N$	–	78.99%
	Total	–	100%

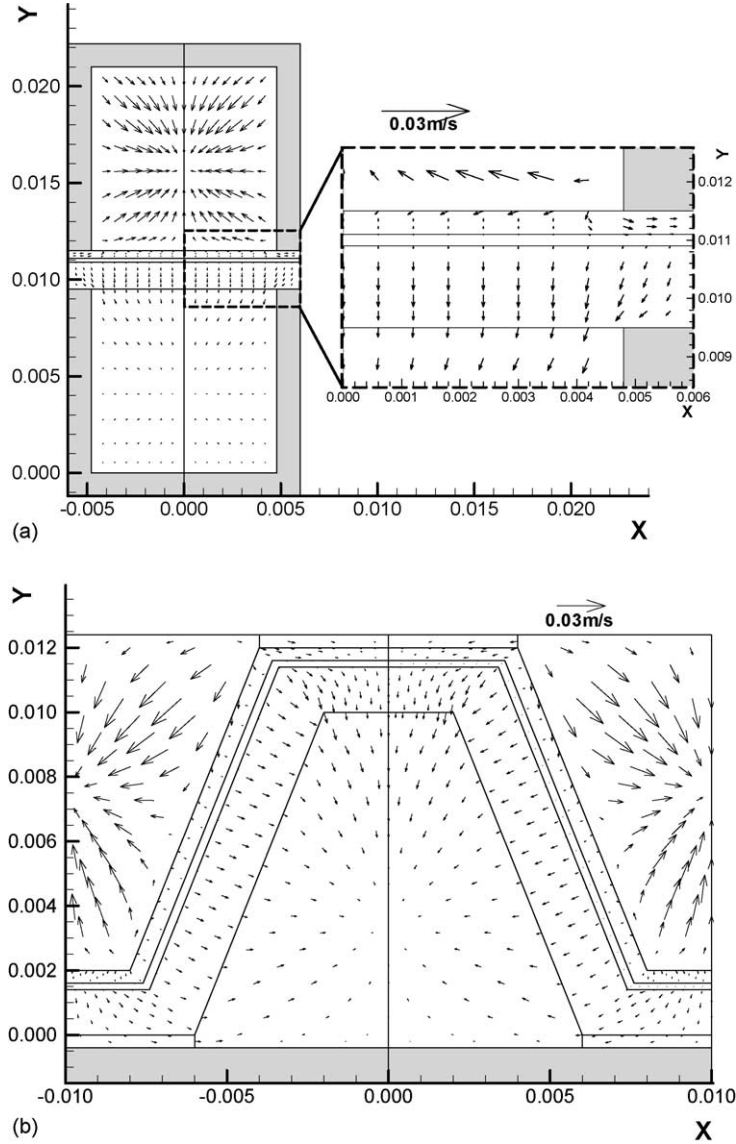


Fig. 3. Comparison of the secondary-flow patterns between the planar and MOLB-type SOFC.

the current passes through electrode can be decomposed two parts, i.e.:

$$\mathbf{i} = \mathbf{i}_C + \mathbf{i}_E \quad (14)$$

$\mathbf{i}_C$  and  $\mathbf{i}_E$  are the currents flowing through the catalyst and the electrolyte, respectively. Since the electrodes are electroneutral everywhere, there is no charge-buildup in the active layers. Thus, the charge conservation is

$$\nabla \cdot \mathbf{i} = 0 \quad (15)$$

That is

$$\nabla \cdot \mathbf{i}_C = -\nabla \cdot \mathbf{i}_E \quad (16)$$

These two current components interact through electrochemical reactions. The electrons are transferred to the catalyst from the electrolyte in the anode, and vice versa in the cath-

ode. Application of Ohm's law to Eq. (16) yields the current conservation:

$$\nabla \cdot (-\sigma_{\text{eff},C} \nabla \Phi_C) = -\mathbf{j}_T \quad (17)$$

$$\nabla \cdot (-\sigma_{\text{eff},E} \nabla \Phi_E) = \mathbf{j}_T \quad (18)$$

where  $\sigma_{\text{eff},C}$  and  $\sigma_{\text{eff},E}$  are the effective electric conductivities of the catalyst and electrolyte, respectively. They are modeled as

$$\sigma_{\text{eff},C} = \sigma_C(1 - \varepsilon)\phi_C p_{i,C} \quad (19)$$

$$\sigma_{\text{eff},E} = \sigma_E(1 - \varepsilon)\phi_E p_{i,E} \quad (20)$$

where  $\phi_C$  and  $\phi_E$  are the volume fraction of the catalyst and electrolyte, respectively.  $p_{i,C}$  is the possibility of the catalyst in the connection of the inter-connector, and  $p_{i,E}$  is the possibility of electrolyte in the connection of PEN plate [12]. It

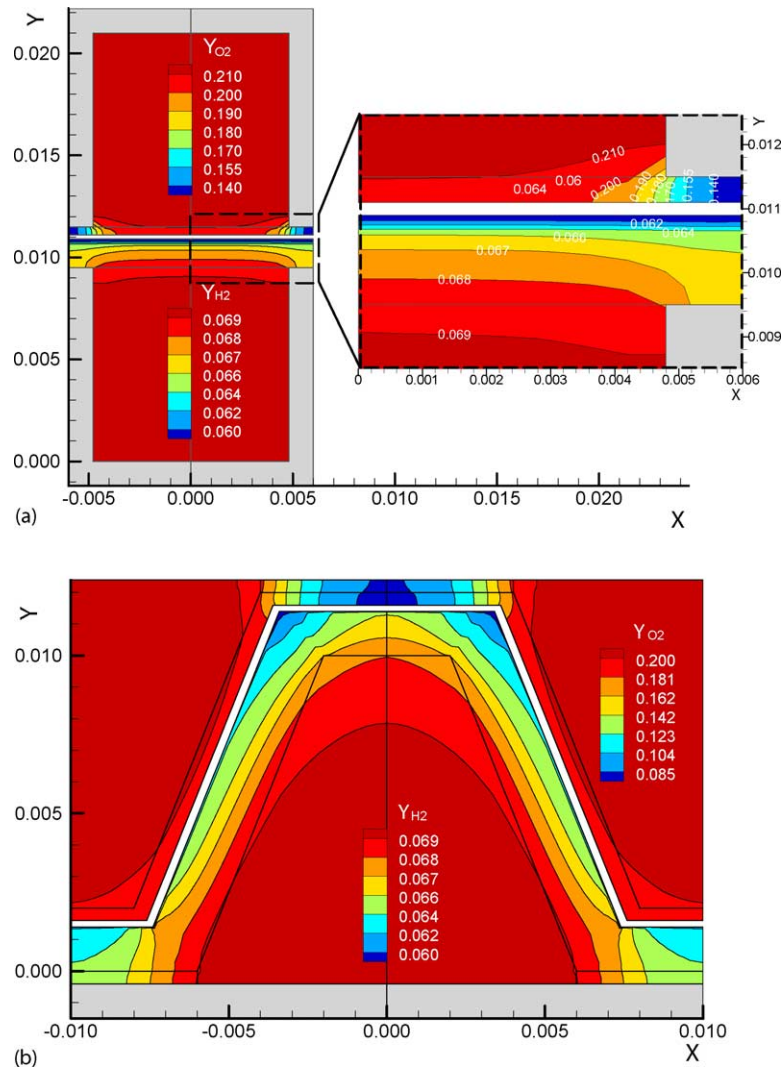


Fig. 4. Mass fraction distributions of the oxygen and hydrogen in the SOFCs: (a) planar SOFC; (b) MOLB-type SOFC.

is noted that only a long-range connection of the same particles stretch from the inter-connector to the electrolyte ensures good conductivity.

### 2.2.3. Geometric parameters and physical properties

Table 1 lists the geometric parameters of the planar SOFC and the MOLB-type SOFC in a single module. To place a common basis, several important parameters are kept at the same value between these two geometries such as the PEN-plate thickness, the channel cross-sectional area and length, and the module volume. The majority of discrepancy between these two designs is the length of the PEN plate. The MOLB-type SOFC has a 16.8 mm PEN plate in length, which is about 40% longer than that of the planar SOFC.

Other parameters and physical properties used in this model are summarized in Table 2. The ambient air supplies the cathode with oxidants. The anode is fed with a simulated reformed gas i.e. a composition of  $\text{CH}_4$ ,  $\text{CO}$ ,  $\text{CO}_2$ ,  $\text{N}_2$ , and  $\text{H}_2\text{O}$ . The molar concentration of the anode fuel

is 45.57/6.97/6.55/36.84/4.07% for  $\text{H}_2/\text{CO}/\text{CO}_2/\text{H}_2\text{O}/\text{CH}_4$ . Among them,  $\text{CH}_4$  and  $\text{N}_2$  are considered as inert gases and serve as diluents. The operation voltage of the cell is set to 0.55 V, meaning that the overpotential within the module is 0.4 V with an OCV of 0.95 V. In addition, the fluid viscosity ( $\mu_{\text{eff}}$ ) is calculated using mixture kinetic theory, specific heat ( $C_p$ ) via JANNAF tables for mixtures, and thermal conductivity ( $k_F$ ) is calculated for constant Prandtl number ( $Pr=0.7$ ).

### 3. Numerical implementation

The governing equations are numerically solved by the control-volume-based finite difference method [13]. The momentum equations are solved, followed by a pressure correction equation that does the mass balance. Species transport equations and electric conduction equations are solved simultaneously after the bulk flow calculation. Velocity control volumes are staggered with respect to the main control volumes, and coupling of the pressure and velocity

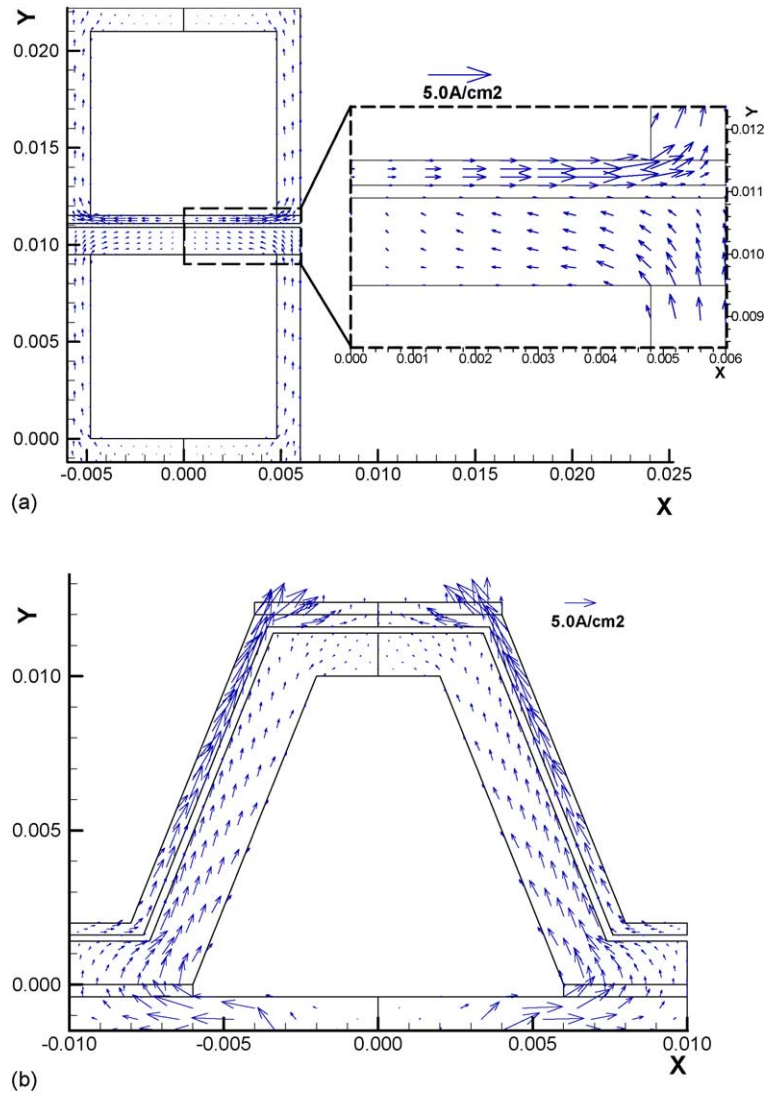


Fig. 5. Current density distributions along the solid-phase of SOFCs: (a) planar SOFC; (b) MOLB-type SOFC.

fields is treated via the SIMPLER pressure correction algorithm [14–16]. Solutions are considered to be converged at each test condition after the ratio of residual source (including mass, momentum, species, and charge) to the maximum flux across a control surface becomes below  $1.0 \times 10^{-6}$ . Computations are performed on structured grids with number of  $12 \times 44 \times 50$  and  $18 \times 40 \times 50$  for the planar SOFC and the MOLB-type SOFC, respectively. Grid-independence test is carried out by running three additional coarser and finer meshes. A typical simulation requires about 300 min of central processing unit time on a Pentium IV 2.8 GHz PC.

## 4. Results and discussion

### 4.1. Secondary flow

Fig. 3 compares the secondary-flow pattern in the flow channel and the porous electrode between the planar SOFC

and the MOLB-type SOFC. The cross-sectional view is cut through the mid-plane of the computational module. Although the structure of the secondary flow between these two geometries is different, the general trend in the movement of the secondary flow is similar in essential. It is briefly described as follows.

In the anode, the secondary flow is directed from the electrolyte toward the flow channel. This is because the gas bulk density in the anode is increased due to the electrochemical oxidation reaction (Eq. (4)). Thus, the outflow should be higher than the inflow in the anode for mass conservation. In contrast, the oxygen reduction reaction in the cathode reduces the air bulk density (Eq. (1)). Thus, the fresh air flows continuously into the cathode from the channel to satisfy the continuity. In the channel flow, the velocity vectors of the secondary flow are always directed toward the channel center due to the wall effect. The stronger secondary flow in the cathode channel is because of the higher inlet velocity of the oxidant.

#### 4.2. Species concentration

A comparison of the distributions of  $Y_{O_2}$  (oxygen) and  $Y_{H_2}$  (hydrogen) between the planar SOFC and the MOLB-type SOFC is shown in Fig. 4. The general trend of the concentration distributions for both types of SOFCs is briefly described as follows. Since the anode/cathode acts a species sink to descend the fuel gas/oxidant, the gradient of species concentration in the both electrodes is significant. In the flow channel, however, the species concentration is relatively uniform. In the cathode of the planar SOFC, a significant gradient of  $Y_{O_2}$  is found in the lateral ( $X$ ) direction. The local minimum of  $Y_{O_2}$  is found in the region in contact with the inter-connector. This is because the fresh air cannot access to this region easily. In the anode of the planar SOFC, the gradient of  $Y_{H_2}$  distribution is significant along the normal ( $Y$ ) direction but no so significant along the lateral direction.

As for the MOLB-type SOFC, the local minimum of  $Y_{O_2}$  is located at the middle of the upper plateau in contact with the inter-connector. The local minimum of  $Y_{H_2}$  occurs at the corner formed by the inclined plane and the ceiling plane where the hydrogen is transported mainly through diffusion.

It is seen from Fig. 4 that the mean concentration of  $H_2/O_2$  in the channel flow of the MOLB-type SOFC is lower than that of the planar SOFC. This means that the fuel/oxidant utilization is higher in the MOLB-type SOFC than that in the planar SOFC. The higher fuel/oxidant utilization is because the longer PEN plate is accompanied by the MOLB-type SOFC. The longer PEN plate provides a more active surface for the electrochemical reaction. The significant fuel utilization will reflect the high current through the fuel cell.

#### 4.3. Electrochemical characteristics

Fig. 5(a) and (b) shows the distributions of the current density along the solid phase of the planar SOFC and the MOLB-type SOFC, respectively. The current is driven from the anode to cathode inside the fuel cell. The arrows indicate the direction as well as the magnitude of the currents. Qualitatively, these two plots have several similar points. First, the current density gradually decreases along its direction in the anode due to the electrochemical oxidation reaction (Eq. (4)). Conversely, the current density gradually increases along its direction in the cathode due to the current accumulation by oxygen reduction reaction (Eq. (1)). Secondly, the anode has a lower current density than the cathode due to its higher area of the current passage. The major difference between these two-type SOFCs is the magnitude of the current density. The MOLB-type SOFC has higher current densities than the planar SOFC.

Fig. 6 compares the overpotential distributions on the active regions between the planar SOFC and the MOLB-type SOFC. In the anode, the positive overpotential directs the transfer current from the catalyst to the electrolyte (Fig. 2(a)), and vice versa in the cathode (Fig. 2(b)). In general, the cathode requires a higher energy to activate the reactants than

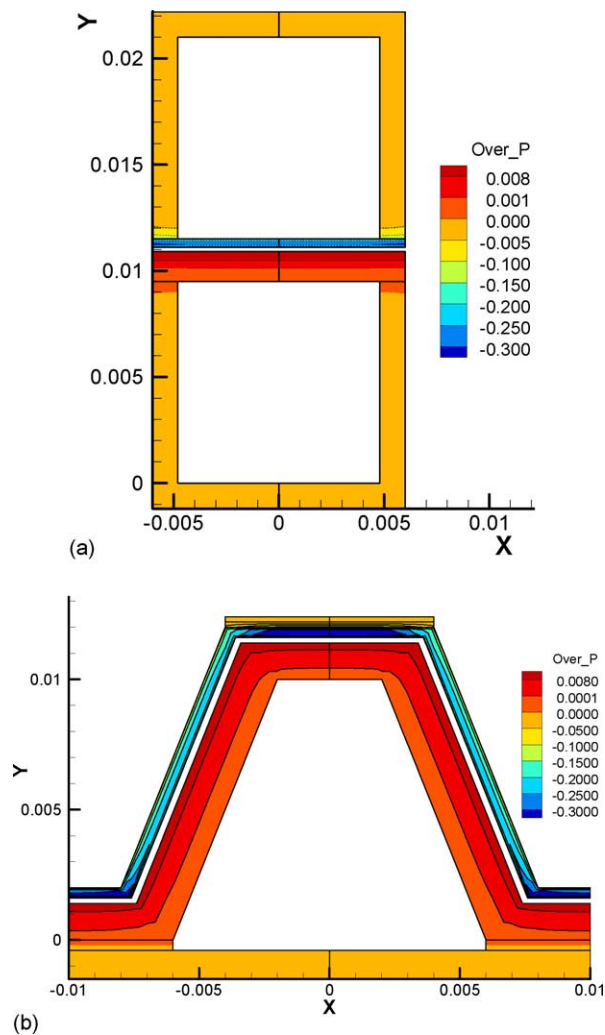


Fig. 6. Overpotential distributions on the surfaces of SOFCs: (a) planar SOFC; (b) MOLB-type SOFC.

the anode. Therefore the absolute value of the overpotential in the cathode is much higher than that in the anode. In addition, it is higher in the region of lower hydrogen/oxygen concentration (Fig. 5). That is depleting the reactants results in increasing the overpotential.

## 5. Conclusions

The present study has made a detailed comparison of the transport and electrochemical characteristics between the planar SOFC and the MOLB-type SOFC. A complete set of conservation equations for mass, momentum, species, energy, and charge are numerically solved with proper account of electrochemical kinetics. The model implements the voltage-to-current algorithm, coupling the potential field with the species concentration field. A realistic spatial variation of electrochemical kinetics is obtained by simultaneously solving the charge transport equations of the catalyst and electrolyte in the electrode for the first time. Informative results

of the reactant gas concentration distribution, overpotential distribution, and current density distribution have been presented and compared. It is found that the MOLB-type SOFC has a higher fuel/oxidant utilization than the planar SOFC due to its longer PEN plate. The significant utilization of the fuel/oxidant reflects the high current passing through the fuel cell.

### Acknowledgments

This work was partly sponsored by the National Science Council of Taiwan under contract no. NSC 92-2212-E-451-002.

### References

- [1] S.P. Simner, J.F. Bonnett, N.L. Canfield, K.D. Meinhardt, J.P. Shelton, V.L. Sprenkle, J.W. Stevenson, *J. Power Sources* 113 (2003) 1–10.
- [2] T. Fukui, S. Ohara, M. Naito, K. Nogi, *J. Power Sources* 110 (2002) 91–95.
- [3] S.P. Jiang, Y.Y. Duan, J.G. Loveb, *J. Electrochem. Soc.* 149 (2002) A1175–A1183.
- [4] V.V. Kharton, E.V. Tsipis, A.A. Yaremchenko, J.R. Frade, *Solid State Ion.* 166 (2004) 327–337.
- [5] T. Ishihara, S. Fukui, H. Nishiguchi, Y. Takita, *J. Electrochem. Soc.* 149 (2002) A823–A828.
- [6] T. Hibino, A. Hashimoto, M. Suzuki, M. Yano, S. Yoshida, M. Sanob, *J. Electrochem. Soc.* 149 (2002) A195–A200.
- [7] Z. Lin, J.W. Stevenson, M.A. Khaleel, *J. Power Sources* 117 (2003) 92–97.
- [8] J.J. Hwang, C.K. Chen, D.Y. Lai, *J. Power Sources*, in press.
- [9] V. Gurau, H. Liu, S. Kakac, *AIChE J.* 44 (1998) 2410–2422.
- [10] J. Bear, J.M. Buchlin, *Modeling and Application of Transport Phenomena in Porous Media*, Kluwer Academic Publishers, Boston, MA, 1991.
- [11] P. Costamagna, K. Honegger, *J. Electrochem. Soc.* 145 (1998) 3995.
- [12] C.H. Kuo, P.K. Gupta, *Acta Metall. Mater.* 39 (1995) 397.
- [13] S.V. Patankar, *Numerical Heat Transfer and Fluid Flow*, Hemisphere, New York, 1980.
- [14] J.P. Van Doormaal, G.D. Raithby, *Numer. Heat Transfer A* 7 (1992) 147–163.
- [15] J.J. Hwang, D.Y. Lai, *Int. J. Heat Mass Transfer* 41 (1998) 979–990.
- [16] J.J. Hwang, C.K. Chen, R.F. Savinell, C.C. Liu, J.C. Wainright, *J. Appl. Electrochem.* 34 (2004) 217–224.